Applied Catalysis B: Environmental 154–155 (2014) 1–8

Contents lists available at ScienceDirect

Applied Catalysis B: Environmental

journal homepage: www.elsevier.com/locate/apcatb

Interactions of plasma species on nickel catalysts: A reactive molecular dynamics study on the influence of temperature and surface structure

W. Somers [a], A. Bogaerts [a], A.C.T. van Duin [b], E.C. Neyts [a,*]

[a] Department of Chemistry, PLASMANT Research Group, University of Antwerp, Universiteitsplein 1, B-2610 Wilrijk-Antwerp, Belgium
[b] Department of Mechanical and Nuclear Engineering, Penn State University, University Park, Pennsylvania 16802, United States

ARTICLE INFO

Article history:
Received 8 November 2013
Received in revised form 25 January 2014
Accepted 30 January 2014
Available online 6 February 2014

Keywords:
Molecular dynamics simulation
ReaxFF
Hydrocarbons
Nickel catalyst
Plasma catalysis

ABSTRACT

Methane reforming by plasma catalysis is a complex process that is far from understood. It requires a multidisciplinary approach which ideally takes into account all effects from the plasma on the catalyst, and vice versa. In this contribution, we focus on the interactions of CH_x ($x = \{1,2,3\}$) radicals that are created in the plasma with several nickel catalyst surfaces. To this end, we perform reactive molecular dynamics simulations, based on the ReaxFF potential, in a wide temperature range of 400–1600 K. First, we focus on the H_2 formation as a function of temperature and surface structure. We observe that substantial H_2 formation is obtained at 1400 K and above, while the role of the surface structure seems limited. Indeed, in the initial stage, the type of nickel surface influences the C–H bond breaking efficiency of adsorbed radicals; however, the continuous carbon diffusion into the surface gradually diminishes the surface crystallinity and therefore reduces the effect of surface structure on the H_2 formation probability. Furthermore, we have also investigated to what extent the species adsorbed on the catalyst surface can participate in surface reactions more in general, for the various surface structures and as a function of temperature. These results are part of the ongoing research on the methane reforming by plasma catalysis, a highly interesting yet complex alternative to conventional reforming processes.

1. Introduction

The Ni-catalyzed reforming of methane is a commonly used process for the production of synthesis gas, a potential clean energy source. However, the associated chemical reactions are strongly endothermic and thus energy-intensive [1]. Combination of plasma and catalysis, so-called plasma catalysis, seems promising. The plasma can activate inert molecules such as CH_4 and induce reactions at reduced temperatures, while the catalyst can increase the selectivity towards specific reaction products. However, plasma catalysis is a technology which is far from understood due to its inherent complexity [2,3]. Indeed, in addition to the inherent complexity of catalysis and the plasma processes taking place, the plasma and catalyst also often demonstrate synergistic effects.

For instance, the presence of the catalyst in the discharge volume affects the retention times of the plasma species in the reactor. Indeed, the plasma species adsorb on the catalyst surface and are therefore longer available to the discharge to interact with other species. This leads to additional reactions and reaction products, which changes the reactive species densities [4,5]. The presence of the catalyst in the discharge volume can also create a so-called packed bed effect, which enhances the electric field. Such an effect, which is also created by adding dielectric materials in the plasma reactor, influences the electron energy distribution function [6,7]. Furthermore, microdischarges may be formed in catalyst pores. All these factors lead to a change in the plasma characteristics, and a concurrent change in the chemistry. In turn, the plasma may reduce the catalyst to increase the catalytic activity. This has for instance been demonstrated for nickel catalysts (with or without a support material), where NiO is reduced to Ni [8]. The plasma also enhances the formation of smaller catalyst nanoparticles, which results in a higher dispersion and thus a larger surface area of the catalyst [9]. Such high catalyst dispersion also reduces coke formation on the catalyst surface [10]. Furthermore, the reactive plasma species can induce several reactions at the catalyst surface, and lower the activation barrier of some reactions. The latter can occur for example in reactions with vibrationally excited species, since they have more energy compared to the ground state of the species.

The interactions between plasma and catalyst described above and their resulting effects demonstrate the complexity of plasma catalysis, and the necessity of a full understanding of these interactions for improving the applicability of this technology. This can

* Corresponding author. Tel.: +32 3 265 23 88; fax: +32 3 265 23 43.
E-mail address: erik.neyts@uantwerpen.be (E.C. Neyts).

0926-3373/$ – see front matter © 2014 Elsevier B.V. All rights reserved.
http://dx.doi.org/10.1016/j.apcatb.2014.01.061

only be accomplished through multidisciplinary research, including both experimental and computational studies.

Recently, a number of studies on such combined effects of plasma and catalyst were performed [6,11–16], although most studies focus on the aspect of the plasma. Both experimental and computational studies on the plasma-based reforming intend to find the optimal working conditions, e.g. to determine which type of discharge is the most advantageous and energy-efficient [17–23]. Mainly cold atmospheric plasmas, like dielectric barrier discharges (DBDs), are being studied. However, warm plasmas, such as gliding arc or microwave discharges, are also investigated in this research field [24–26]. From the catalytic point of view, various experimental studies describe the adsorption and decomposition of CH_4 on nickel catalysts [27–29]. Furthermore, Density Functional Theory (DFT) calculations were performed to further describe these processes [30,31]. In addition to the DFT calculations, classical molecular dynamics (MD) simulations were done to describe the dissociation of methyl radicals adsorbed on nickel surfaces [32,33]. Ab initio MD simulations on the initial stages of the growth of carbon nanotubes and graphene also investigate the adsorption and dehydrogenation of CH_4 on nickel surfaces, albeit at higher temperatures (1500 K) [34]. The studies mentioned above include species derived from CH_4, that are also formed in plasmas, and insight in the interactions of these species with catalyst surfaces can contribute to a more fundamental understanding of methane reforming through plasma catalysis.

In our previous work [33], we focused on the interactions of CH_x ($x = \{1,2,3\}$) radicals with several nickel surfaces at a temperature of 400 K, i.e. a typical temperature of a DBD. By performing MD simulations, using the Reactive Force Field (ReaxFF) potential [35], we found that the surface type influences the C–H bond breaking after adsorption as well as the reactivity towards formation of CH_x and C_2H_x species [33]. Little H_2 formation was observed at 400 K. Thus, a temperature study with the emphasis on H_2 formation was performed on Ni(1 1 1), in the temperature range of 400–1600 K [36]. This maximum temperature is for example reached in the transitional regime of a gliding arc discharge. A substantial number of H_2 molecules were indeed formed after CH_x impacts at 1400 and 1600 K. However, these high temperatures also induce the diffusion of C-atoms into the nickel surface, which is more desired for e.g. (plasma-)growth of carbon nanotubes [37] or graphene [38] than for a reforming reaction. It would be more interesting to obtain significant H_2 formation, with less carbon diffusion. Since the type of nickel surface influences the reactivity at 400 K, we should consider the role of the nickel surface on the H_2 formation and carbon diffusion at higher temperatures as well.

In this work, we therefore first investigate the direct H_2 formation on the catalyst surface for five different nickel surfaces, in the temperature range of 400–1600 K. Subsequently, we will also try to obtain a more general insight in the temperature effect on the reactivity of adsorbed plasma species.

2. Computational details

The reaction behavior of the CH_x ($x = \{1,2,3\}$) radicals on the catalyst surface is described with molecular dynamics (MD) simulations, based on the ReaxFF potential [35]. ReaxFF has been applied to a wide variety of systems, including silicon oxides [39], biochemical systems [40] and hydrocarbons [35]. For this work, we used parameters for the Ni/C/H set developed and validated by Mueller and coworkers [32]. Previously, we validated this force field for our purposes, and successfully applied it in our earlier studies on plasma catalysis [33,36], carbon nanotube growth [41–43] and graphene growth [38], demonstrating the wide application range of the Ni/C/H force field. The computational setup is the same as used in our previous studies [33,36]. A detailed description of the force field can be found in [44].

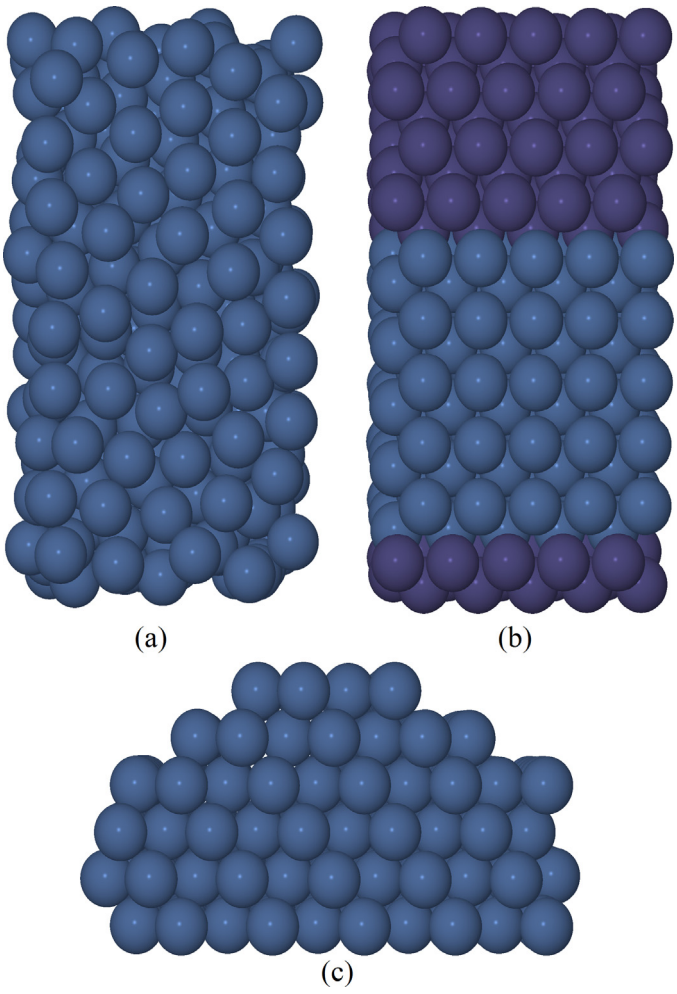

Fig. 1. Top view of (a) aNi, (b) pNi, for which the dark blue spheres represent the (1 1 1) facet and the light blue spheres the (1 0 0) facet, and side view of (c) sNi.

For this study, we constructed five different nickel surfaces, namely: Ni(1 1 1), Ni(1 0 0), a step-edged Ni(1 1 1) surface (denoted as sNi), an amorphous surface (aNi) and a polycrystalline surface (pNi). The first three surfaces were already used in our previous work to study the influence of surface energy and step-edges in the surface on the adsorption probability of the radicals and the reactions after adsorption [33]. However, the crystallinity of the surface might change due to the interactions with the plasma. Consequently, this can alter the reactivity of the catalyst. For this reason, aNi and pNi are included in this study, to elucidate this effect of change in crystallinity. The flat surfaces, i.e. Ni(1 1 1), Ni(1 0 0) and pNi, each consist of 300 Ni-atoms, equally divided over 6 atomic layers. The pNi structure shows a (1 1 1) facet and a (1 0 0) facet. The amorphous surface also has 300 atoms, randomly distributed in the cell volume such that separate layers are difficult to distinguish. Finally, the sNi surface is created with 255 atoms, divided over 6 layers in a manner that step-edges are present in the surface. The structure of this surface is shown in Fig. 1, together with those of aNi and pNi. The full structures of Ni(1 1 1) and Ni(1 0 0) can be found in our previous work [33], while the (1 1 1) and (1 0 0) facet can also be seen in Fig. 1b.

Prior to the impacts, all the surfaces were equilibrated to the desired temperature, in the range of 400–1600 K, employing the Bussi thermostat with a coupling constant of 100 ps [45]. Subsequently, both single and consecutive impacts of CH_x radicals on

the nickel surfaces were performed, again applying the Bussi thermostat. The single impacts provide information concerning the C–H bond breaking after adsorption, while the consecutive impacts mimic a continuous hydrocarbon flux towards the surface, and describe the formation of new species as a consequence of bond breaking and recombination reactions. For both types of impacts, the radicals are added to the system at a z-position of 10 Å above the top-layer of the nickel surface, while the initial $\{x,y\}$ coordinates are randomized. The initial velocity vector of the impinging particle is also randomized. Periodic boundary conditions are applied in the $\{x,y\}$ directions, to simulate a semi-infinite surface.

Each single impact is performed on a pristine nickel surface, for a total simulation time of 5 ps, at temperatures of 400 K, 800 K, 1200 K and 1600 K. Within this time, the radical is reflected or adsorbed, and after the latter case C–H bond breaking can occur. The single impact of each type of radical on each of the five surfaces at each of the four different temperatures, i.e. a total of 60 simulations cases, was repeated 500 times, to obtain statistically reasonable results.

In the case of the consecutive impacts, each impact is followed for 6.25 ps, at temperatures of 400 K, 800 K, 1000 K, 1200 K, 1400 K and 1600 K. The resulting surface is subsequently used as input configuration for the next impact. Therefore, the impacting radicals are not only adsorbed or reflected, but they can also react with previously adsorbed radicals. As a result, new species are formed, which are removed from the system if they desorb from the surface. This procedure is repeated 150 times for the CH_3 impacts, and 250 times for the CH_2 and CH impacts. The higher number of simulated CH_2 and CH impacts is required due their higher reactivity after adsorption, so that more impacts are needed to obtain clear trends. For each case, i.e., for each sequence of impacts of each type of radical on each of the five surfaces at each of the six different temperatures, three simulations were performed, leading to a total of 270 consecutive impacts simulations (each consisting of 150 impacts for CH_3 and 250 impacts for CH_2 and CH). The reported results are the averages over the three simulations per case, with the associated standard deviations.

3. Results and discussion

3.1. Effect of temperature and nickel surface structure on H_2 formation

In our previous work, we illustrated that hardly any H_2 is formed after CH_x impacts at a temperature of 400 K, regardless the type of nickel surface on which the radicals impinge [33]. Further studies on Ni(1 1 1) showed that a temperature increase towards 1400 K or higher is required for substantial formation of H_2 [36]. However, at 400 K, the surface type does influence the C–H bond breaking and the reactivity towards formation of CH_x and C_2H_x species. If this dependency between reactivity and surface type is maintained at high temperatures, this might influence the number of formed H_2 molecules after impacts on the different nickel surfaces.

The influence of both the temperature and the specific nickel surface structure on the average number of broken C–H bonds after adsorption of a CH_x radical is shown in Fig. 2. The temperature influence on the C–H bond breaking is the highest for adsorbed CH_3 radicals. At 400 K, adsorbed CH_3 radicals remain kinetically stable and only rarely a C–H bond is broken. As the temperature increases towards 800 K, the bond breaking starts to occur more often. Further heating has even a greater effect, as illustrated in Fig. 2a. However, the reactivity is still low, since at the highest temperature of 1600 K, at maximum 1.14 out of three C–H bonds are broken after adsorption. For the CH_2 and CH radicals, there is already sufficient bond breaking at 400 K and 800 K. This is still promoted by increasing the temperature, but not to the same extent

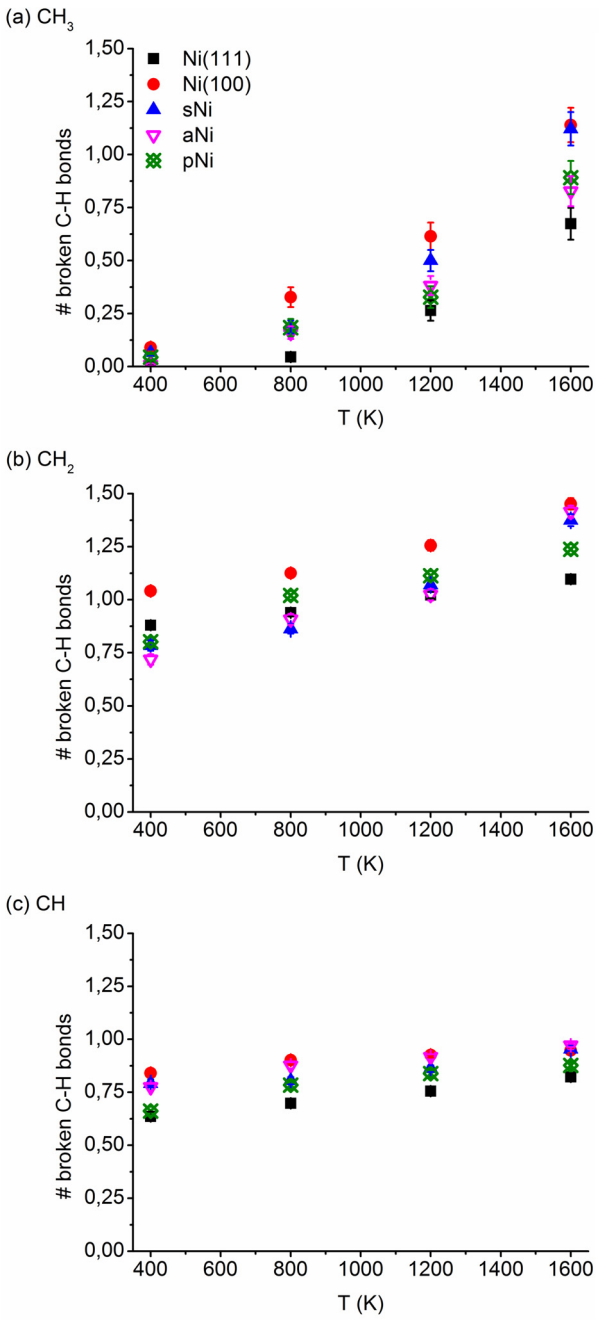

Fig. 2. Average number of broken C–H bonds after adsorption of a single (a) CH_3, (b) CH_2 and (c) CH radical (i.e., after non-consecutive impacts) as a function of temperature and for various surface structures. The error bars represent the standard deviation of the average, calculated over 500 simulations.

as for the CH_3 radicals. The highest reactivity is obtained for the CH radicals, since about 75% of the adsorptions are followed by breaking of the one C–H bond. The reactivity of the CH_2 radicals lies between that of CH and CH_3, with a maximum number of broken C–H bonds varying from about 0.75–1.00 at 400 K to around 1.25 out of 2 C–H bonds at 1600 K.

If we now consider the role of the nickel surface, clear differences between the five surfaces are observed. The Ni(1 1 1) surface, which is the most stable Ni-surface, has the lowest reactivity over the investigated temperature range for each type of radical. In contrast, the higher energy Ni(1 0 0) surface clearly promotes C–H bond breaking. Furthermore, the results for the polycrystalline structure are as expected, namely between those of Ni(1 0 0) and Ni(1 1 1),

since pNi contains both structures. As discussed in our previous work, the presence of step-edges on Ni(1 1 1) improved the reactivity at 400 K; the same is now observed at higher temperatures, for which sNi is amongst the most reactive surfaces. Finally, the number of broken C–H bonds on aNi is mostly located between the results of the other surfaces. This implies that the loss of crystallinity does not immediately lead to lowering of the reactivity. Overall, the influence of the surface on the C–H bond breaking is the most significant for the CH_3 radicals, where the number of broken C–H bonds per impact rises from 0.67 on Ni(1 1 1) to 1.14 on Ni(1 0 0) at 1600 K, hence a difference of 0.47 broken C–H bonds per impact. For the same temperature, this difference is 0.36 and 0.12 broken C–H bonds for the CH_2 and CH radicals, respectively. Although the influence of temperature and surface structure is the highest for the CH_3 radicals, the reactivity is still the lowest compared to the other radicals.

These results indicate the role of the surface structure in creating H-atoms bound to the nickel surface. During consecutive impacts, these H-atoms can react with other incoming radicals or recombine with each other into H_2. Since most C–H bond breaking occurs on Ni(1 0 0), we would expect that more H_2 is formed after impacts on this surface. However, the expected trend is not observed in the results of the consecutive impacts, as shown in Fig. 3. In case of the CH_3 radicals (see Fig. 3a), roughly two H_2 molecules are formed after 150 impacts on Ni(1 0 0), with hardly any temperature dependency. Furthermore, the difference between the surfaces remains small, at least at temperatures up to 1200 K. The first significant difference between the surfaces is obtained at 1400 K, while at 1600 K, a clear separation between the values is obtained. For this latter temperature, sNi has the highest selectivity towards H_2 and Ni(1 0 0) the lowest selectivity. While the stepped Ni(1 1 1) surface yields a similar number of broken C–H bonds after adsorption of a CH_3 radical as the Ni(1 0 0) surface (see Fig. 2a), five times more H_2 molecules are formed on the sNi surface. Therefore, there must be other factors that affect the H_2 formation. Indeed, besides recombining to H_2, the adsorbed H-atoms can also react with the incoming CH_3 radicals, or diffuse into the surface. The interaction with incoming CH_3 is found to be very similar on all investigated surfaces. The diffusion of H-atoms, on the other hand, turns out to be surface dependent. The H-diffusivity is the highest for Ni(1 0 0), and hence less H-atoms remain available on this surface to form H_2. Since both Ni(1 1 1) and sNi have the same orientation, they also have a similar H-diffusivity. These observations are consistent with the more open surface packing of the Ni(1 0 0) surface in comparison with the close-packed Ni(1 1 1) surface structure (cf. Fig. 1), rendering H-diffusion into Ni(1 0 0) kinetically more favorable. The difference in H_2 formation on the Ni(1 1 1) and sNi surfaces is therefore determined by the C–H bond breaking probability, which is indeed higher on sNi, as illustrated in Fig. 2a. The H-diffusion on pNi and aNi, as well as the number of broken C–H bonds after adsorption, is a little higher than on Ni(1 1 1) at 1600 K. Hence, the combination of these two opposite factors results in a similar number of H_2 molecules formed on pNi, aNi and Ni(1 1 1).

In case of the CH_2 and CH impacts, the difference in H_2 formation between the surfaces is again observed mainly at higher temperatures, i.e. starting from 1400 K for CH_2, or 1200 K for CH. Remarkably, sNi is the surface with the lowest selectivity towards H_2 formation after 250 impacts under these conditions (see Fig. 3b and c), although it still has a relatively high number of broken C–H bonds and the lowest H-diffusivity. Apparently, these two factors are not sufficient to explain the observed differences, and other aspects need to be taken into account. One of these aspects is the formation of other CH_x and C_2H_x species, which also reduces the number of H-atoms on the surface available for H_2 formation. However, there is no clear dependency between this aspect and the H_2 formation. For instance, both Ni(1 1 1) and sNi show the most abundant CH_x formation and a similar H-diffusivity during the consecutive CH_2 impacts, but the H_2 formation seems more probable on Ni(1 1 1) than on sNi, in spite of the lower C–H bond breaking probability on Ni(1 1 1). Another factor that was taken into account is the diffusion rate of the H-atoms over the surface. If the diffusion rate is indeed dependent on the surface structure, the H-atoms will cover different distances over the different surfaces within the same simulation time. The longer the distance travelled by the H-atoms, the higher the probability of encountering another

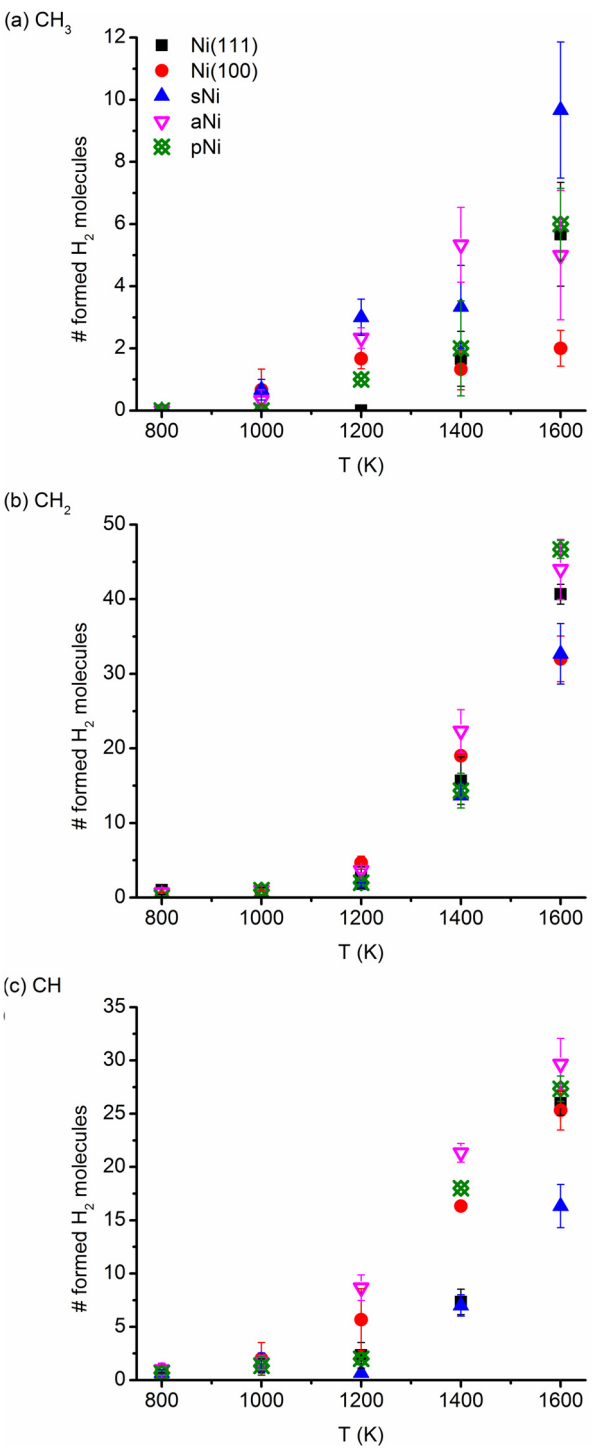

Fig. 3. Average number of formed H_2 molecules, and associated standard deviations over the three simulations, after consecutive impacts of (a) 150 CH_3, (b) 250 CH_2 and (c) 250 CH radicals as a function of temperature and for various surface structures.

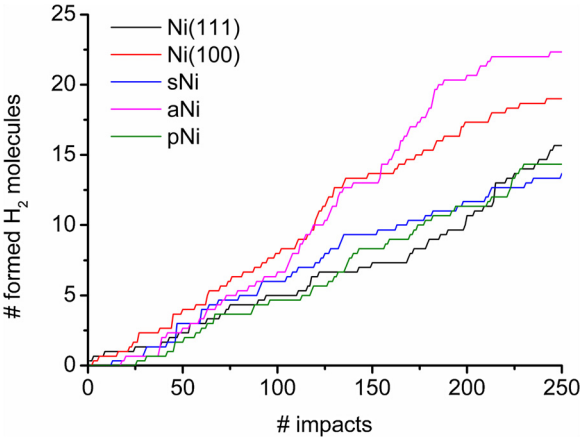

Fig. 4. Average number of formed H_2 molecules as a function of the number of CH_2 impacts on the different surfaces at 1400 K.

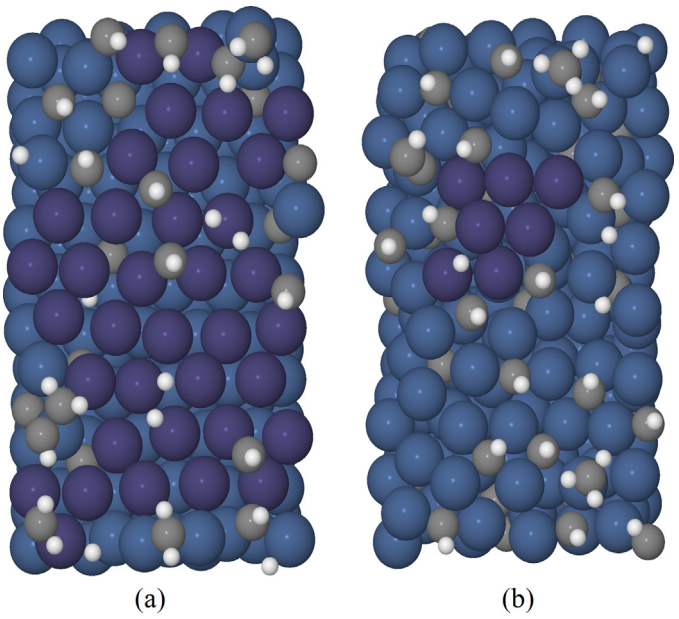

Fig. 5. Top view of the Ni(1 1 1) surface after (a) 50 and (b) 125 consecutive CH_2 impacts at 1400 K. The dark blue spheres represent the (1 1 1) facet in the top-layer.

H-atom and recombining to H_2. Comparison of the diffusion rate over the entire temperature range, however, shows that the differences between Ni(1 1 1) and Ni(1 0 0) are too small to explain the dissimilarities in H_2 selectivity between both surfaces. Finally, the role of the number of adsorbed C-atoms was considered. Each adsorbed C-atom can undergo C–H bond breaking; therefore, more adsorptions can lead to more H-atoms on the surface. After 250 consecutive CH_2 and CH impacts, no correlation between H_2 formation and the number of adsorbed C-atoms is found for most cases. However, the low H_2 selectivity of sNi during the CH_2 and CH impacts (see Fig. 3b and c) can be a consequence of the much lower number of adsorbed C-atoms on this surface compared to the other surfaces. Indeed, there are about 7 and 14 adsorbed C-atoms less on sNi, after the CH_2 and CH impacts, respectively. Furthermore, the influence of steps in the surface on the C–H bond breaking is the highest for the adsorbed CH_3 radicals, while the difference with the other surfaces is much smaller for the CH_2 and CH radicals, as shown in Fig. 2. This decrease in difference between the surfaces of the C–H bond breaking probability, together with the decrease in the number of adsorbed C-atoms leads to the lower H_2 formation. This correlation between H_2 formation and the number of adsorbed C-atoms, however, is only observed for sNi.

Since there are no clear explanations for the different H_2 selectivities at temperatures of 1400 K and higher in the case of CH_2 and CH impacts, we need to consider whether it is still correct to distinguish the surfaces from each other at these temperatures. In our previous work, we already illustrated that at such temperatures, the carbon diffusion in Ni(1 1 1) becomes a dominant process, with diffusion into the lower-lying Ni-layers [36]. The same is observed for the other surfaces, especially after the CH_2 and CH impacts. This diffusion eventually leads to a loss of the crystallinity in the top-layers of the surface, since more and more C-atoms are positioned between the Ni-atoms. At this point, the formation of new H_2 molecules cannot be fully allocated to the initial surface structure, since the latter is not maintained anymore.

In Fig. 4, the H_2 formation at 1400 K is followed on the different surfaces as a function of the number of CH_2 impacts. As illustrated already in Fig. 3b, there is a considerable difference in the number of H_2 molecules formed after 250 impacts. However, after approximately 100–125 impacts, the maximum difference is only 5 H_2 molecules. Note that these impacts are followed by C-diffusion, but certain regions of the top-layer still maintain their crystallinity. This is illustrated for Ni(1 1 1) in Fig. 5, for which the top-layer exists mostly out of the (1 1 1) facet after 50 CH_2 impacts. This crystallinity gradually decreases during the following impacts, resulting in only a small (1 1 1) facet after 125 impacts. However, up to this point, the observed differences in H_2 formation can still be explained by the C–H bond breaking probability and the H-diffusivity, combined with the total number of adsorbed C-atoms and the loss of H-atoms in reactions (excluding H_2 formation). While these last two factors did not show an obvious dependency with the H_2 formation after 250 impacts, except for the adsorbed C-atoms on sNi, their role is more clear for the first 125 impacts. After 125 CH_2 impacts, both Ni(1 0 0) and aNi have the same number of adsorbed C-atoms, and the same loss of H-atoms due to diffusion or reactions. However, the C–H bond breaking after adsorption is slightly higher for Ni(1 0 0), hence the slightly higher H_2 formation for the first 100–125 impacts. For pNi, both the total number of adsorbed C-atoms as the C–H bond breaking probability are lower than for Ni(1 0 0) and aNi, while the same number of H-atoms are lost. This results in the lower number of formed H_2 molecules. The Ni(1 1 1) surface has the lowest C–H bond breaking probability, and the lowest number of adsorbed C-atoms, hence this explains its low H_2 selectivity after 125 impacts. The only difference between Ni(1 1 1) and sNi at this point is the higher C–H bond breaking for sNi, therefore, more H_2 is formed on this surface than on Ni(1 1 1).

However, during the next 125 impacts more carbon is added to the surface, and the continued diffusion of C-atoms into the subsurface and bulk reduces the crystallinity in the top-layers. As a consequence, the correlation between H_2 formation and the type of nickel surface becomes unclear, since the trends of the first 125 impacts are not maintained anymore. Gradually, aNi becomes the most H_2 selective surface, and the reactivity of Ni(1 1 1) starts to increase more rapidly. Especially the latter case is curious, since less C-atoms are adsorbed on Ni(1 1 1) than on aNi, and the C–H bond breaking after adsorption is the lowest for Ni(1 1 1). However, this C–H bond breaking was determined with single, non-consecutive impacts on a pristine nickel surface. During the consecutive impacts, the bond breaking occurs on a less crystalline surface with adsorbed C- and H-atoms on it, which will influence the initial bond breaking probability. Additionally, the increased diffusion during the last 125 impacts also influences the C–H bond breaking, since it further changes the crystallinity. Therefore, the C–H bond breaking probability might alter during the impacts, dependent of surface structure and C-diffusion. This makes it difficult to estimate which surface has the highest C–H bond breaking

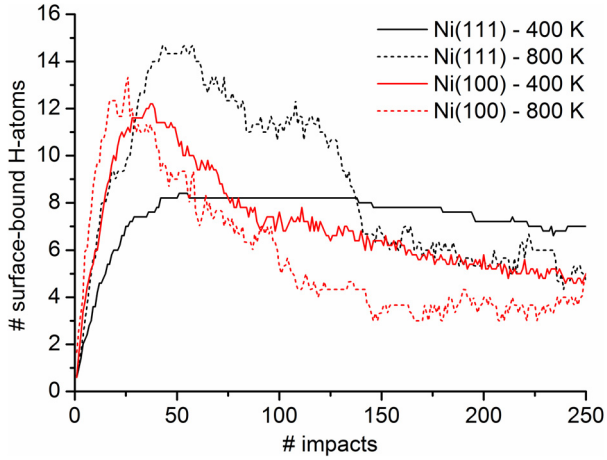

Fig. 6. Average number of surface-bound H-atoms as a function of the number of CH_2 impacts for Ni(1 1 1) and Ni(1 0 0) at 400 and 800 K.

probability. Furthermore, the alteration in C–H bond breaking probability and surface structure is different for each simulation, hence giving rise to deviations between the simulations, which are difficult to define. This implies that, despite the fact that all surfaces are amorphous after 250 impacts, each surface still has a particular (amorphous) structure, different from the other surfaces. Therefore, each of these amorphous surfaces has its own reactivity, which results in different hydrogen formation rates for the various surfaces. We conclude that the nickel surface structure initially (strongly) influences the reactivity after adsorption, but that the effect on the long-term reactivity is limited, due to loss of the crystallinity and change of the C–H bond breaking probability.

3.2. *Effect of temperature and nickel surface structure on the reactivity of adsorbed H-atoms*

In the previous section, we focused on the influence of the nickel surface structure on the H_2 formation. As shown in Fig. 3, and as described in our previous work [36], substantial H_2 formation is obtained at temperatures of 1400 K and above at all Ni surfaces. For processes focusing on the catalytic synthesis of H_2, our simulations predict that this is the required temperature regime. However, in plasma systems, H_2 is also formed through several reactions in the gas (plasma) phase, involving radicals, electrons and ions. This includes the three-body recombination reaction among two H-atoms, with a gas molecule as third body, as well as several other chemical reactions of H-atoms with hydrocarbons [22]. Moreover, besides the formation of H_2, the reactions between H-atoms and hydrocarbons can also form other hydrocarbon species [22]. In plasma catalysis, H-atoms are not only present in the gas phase, but they are also adsorbed on the catalyst surface. Therefore, it is important to know in general to what extent adsorbed H-atoms can participate in reactions with incoming radicals or other adsorbed species and subsequently desorb from the catalyst surface.

Previously, we demonstrated that at a temperature of 400 K, the H-atoms adsorbed on Ni(1 1 1) after CH_2 impacts rarely react with incoming radicals, while this reaction does occur on the other surfaces [33]. As shown in Fig. 6, a temperature increase to 800 K is already sufficient to activate the adsorbed H-atoms on Ni(1 1 1) to react with incoming radicals and form new molecules (i.e. mostly hydrocarbons and little H_2, as was demonstrated in [36]). Indeed, at first, the impacts lead to adsorption and dissociation of CH_2, which generates adsorbed H-atoms, but the number of adsorbed H-atoms subsequently decreases as they react with the incoming radicals. This is in contrast to the behavior at 400 K for Ni(1 1 1), where

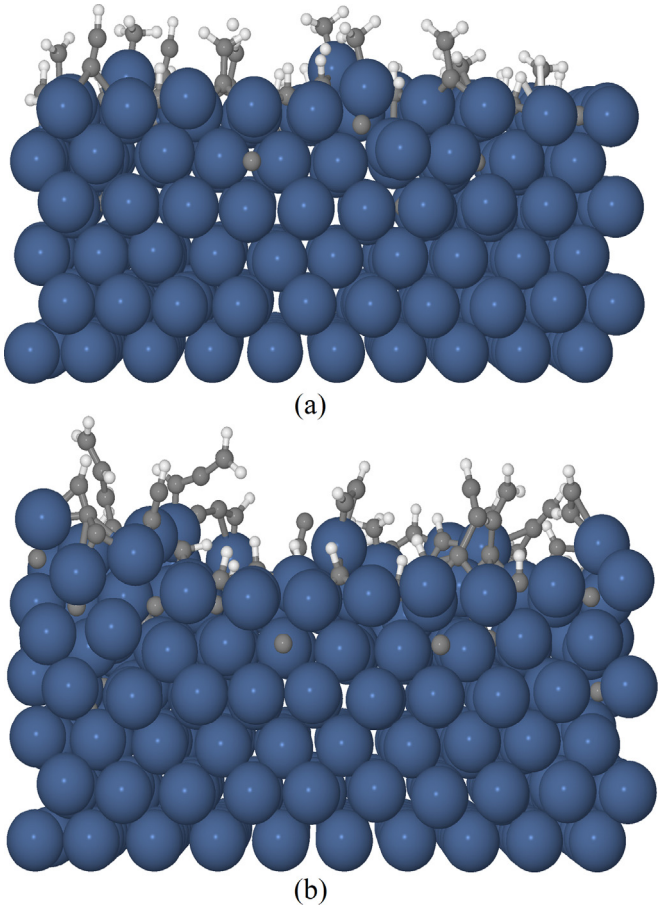

Fig. 7. Side view of Ni(1 0 0) after 250 (a) CH_2 and (b) CH impacts at 800 K.

the number of surface-bound H-atoms remains constant, indicating that the H-atoms do not react with incoming radicals to form new products (such as hydrocarbons or H_2 molecules). However, the incoming radicals do react with other species adsorbed on the Ni(1 1 1) surface, such as CH_2 and CH, which leads to the formation of hydrocarbons. For the other surfaces investigated, the surface bound H-atoms already participate in recombination reactions at 400 K, and a temperature increase has less effect, as illustrated for Ni(1 0 0) in Fig. 6.

Furthermore, performing the impacts at a temperature of 800 K instead of 400 K hardly influences the total number of adsorbed C-atoms after the CH_x impacts, and the diffusion of C-atoms into the nickel surface remains low, as illustrated in Fig. 7. Therefore, we expect a similar (limited) amount of coke formation at 400 and 800 K. Further increasing the temperature leads to additional adsorption of C-atoms, as shown for Ni(1 0 0) in Fig. 8. This is due to the promoted diffusion of C-atoms into the surface at such high temperatures (cf. previous section), which regenerates areas for adsorption in the top-layer.

As discussed earlier, carbon deposition can reduce the performance of the catalyst in the reforming process [36]. If the focus lies on the catalytic synthesis of H_2 or the growth of carbon nanotubes, temperatures of 1400 K and above are appropriate. However, for optimizing the reforming process, and more specifically the catalyst lifetime, lower temperatures are preferred to avoid catalyst deactivation by coke deposition and sintering [46]. At temperatures of 1200 K and above, a large number of adsorbed C-atoms diffuse into the nickel surfaces. Within the current timescale, no accumulation of the C-atoms or polymerization of C_nH_m radicals on the surface is observed. Such processes deactivate the catalyst and are most likely

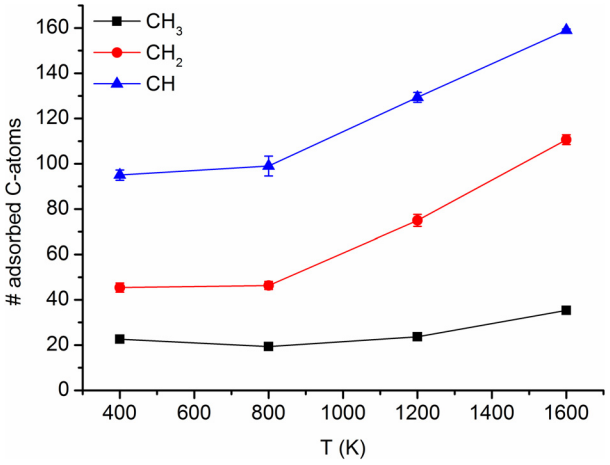

Fig. 8. Average number of adsorbed C-atoms on Ni(1 0 0) after consecutive impacts of the three radicals as a function of temperature.

to occur at high temperatures. However, the fact that these processes are not observed is most probably related to the short time scales of the simulations. As stated before, the carbon diffusion into the surface is low in the range of 400–800 K, so a limited amount of coke formation is expected. Furthermore, the results discussed above indicate that a temperature of 800 K is sufficient to induce interactions between plasma species and H-atoms adsorbed on the various nickel surfaces studied in this work. Even at 400 K, these interactions already occur, although less frequently on Ni(1 1 1). In view of this observation, and keeping in mind the multiplicity of reactions in the plasma, the combination of plasma technology and catalysis for methane reforming seems already promising in the temperature range of 400–800 K. The carbon diffusion, and possible coke formation, remains low in this temperature range, while all the adsorbed species interact with the incoming radicals. Obviously, in a plasma system, additional species besides the studied CH_x radicals are present (e.g. other radicals, excited species, . . .), which can further enhance the reactivity in this temperature range.

4. Summary and conclusions

Reactive molecular dynamics simulations, using the ReaxFF potential, were carried out to investigate the interactions of impacting CH_x ($x = \{1,2,3\}$) radicals on nickel catalyst surfaces as a function of temperature and surface structure.

After adsorption of a single CH_x radical, the subsequent C–H bond breaking depends on both the temperature and exact surface structure. At higher temperature, more C–H bonds get broken upon impact of CH_x radicals. The temperature influence on the bond breaking process after adsorption is the highest for CH_3, which is kinetically stable at low temperatures (i.e. 400 K), followed by CH_2 and CH. Furthermore, there is an increased C–H bond breaking for each type of radical on Ni(1 0 0) and sNi, compared to Ni(1 1 1). These two surfaces have a higher surface energy or step-edges in the structure compared to the stable Ni(1 1 1) surface. The results for pNi, which is partially (1 1 1) and (1 0 0) oriented, are between those of Ni(1 1 1) and Ni(1 0 0), as expected. More importantly, an amorphous structure does not lead to lowering of the reactivity, since the reactivity on aNi appears to be located between those of the other surfaces.

Remarkably, the surfaces which promote the C–H bond breaking are not necessarily the most selective towards H_2 formation after consecutive impacts of the radicals at high temperatures, i.e., 1400 K and above. For the CH_3 impacts, the observed differences can be attributed to the H-diffusivity into the surface. This diffusivity is highest for Ni(1 0 0), and hence less H-atoms are available to recombine into H_2. However, for the CH_2 and CH radicals, for which the reactivity after adsorption is much higher, no clear correlation between surface structure and H_2 formation is found. This is attributed to a loss of crystallinity induced by the diffusion of multiple C-atoms into the surface. The top-layer of the different surfaces loses its initial structure; hence a proper distinction between the surfaces cannot be made anymore. We therefore conclude that the nickel surface structure initially influences the C–H bond breaking, and therefore the H_2 formation, but as the carbon diffusion in the surface increases, the role of the surface structure seems to become limited.

It is demonstrated that the H_2 formation at the catalyst surface requires temperatures in the order of 1400 K. However, in plasma catalysis, the plasma also contributes to the H_2 (and hydrocarbon) formation, by reactions involving radicals, electrons and ions. Since reactions with H-atoms in the plasma can lead to the formation of H_2 or hydrocarbons, the extent to which adsorbed H-atoms at the catalyst surface desorb and further react in the plasma can also be of importance. Only on Ni(1 1 1), the adsorbed H-atoms rarely react with incoming radicals at a temperature of 400 K. Increasing the temperature to 800 K overcomes this limitation. At the other surfaces, the adsorbed H-atoms can already react with incoming radicals at 400 K as well. Furthermore, the total number of adsorbed C-atoms remains almost the same at 400 and 800 K for all surfaces. We conclude that methane reforming by plasma catalysis seems promising in this temperature range, since the reactivity of the adsorbed species is already fairly high, and the diffusion of C-atoms into the surface remains low.

Acknowledgments

This work was carried out in part using the Turing HPC infrastructure at the CalcUA core facility of the Universiteit Antwerpen (UA), a division of the Flemish Supercomputer Center VSC, funded by the Hercules Foundation, the Flemish Government (department EWI) and the UA.

References

[1] J.R.H. Ross, Catal. Today 100 (2005) 151–158.
[2] S. Samukawa, et al., J. Phys. D: Appl. Phys. 45 (2012) 253001.
[3] K. Ostrikov, E.C. Neyts, M. Meyyappan, Adv. Phys. 62 (2013) 113–224.
[4] H.L. Chen, H.M. Lee, S.H. Chen, M.B. Chang, S.J. Yu, S.H. Li, Environ. Sci. Technol. 43 (2009) 2216–2227.
[5] H.L. Chen, H.M. Lee, S.H. Chen, Y. Chao, M.B. Chang, Appl. Catal. B: Environ. 85 (2008) 1–9.
[6] X. Tu, H.J. Gallon, J.C. Whitehead, J. Phys. D: Appl. Phys. 44 (2011) 482003.
[7] H.-H. Kim, A. Ogata, Eur. Phys. J. Appl. Phys. 55 (2011) 13806.
[8] H.J. Gallon, X. Tu, M.V. Twigg, J.C. Whitehead, Appl. Catal. B: Environ. 106 (2011) 616–620.
[9] C.-j. Liu, J. Zou, K. Yu, D. Cheng, Y. Han, J. Zhan, C. Ratanatawanate, B.W.-L. Jang, Pure Appl. Chem. 78 (2006) 1227–1238.
[10] R. Martínez, E. Romero, C. Guimon, R. Bilbao, Appl. Catal. A: Gen. 274 (2004) 139–149.
[11] T. Nozaki, K. Okazaki, Catal. Today 211 (2013) 29–38.
[12] X. Tu, H.J. Gallon, J.C. Whitehead, Catal. Today 211 (2013) 120–125.
[13] H.J. Gallon, X. Tu, J.C. Whitehead, Plasma Process. Polym. 9 (2012) 90–97.
[14] X. Tu, J.C. Whitehead, Appl. Catal. B: Environ. 125 (2012) 439–448.
[15] A.-J. Zhang, A.-M. Zhu, J. Guo, Y. Xu, C. Shi, Chem. Eng. J. 156 (2010) 601–606.
[16] H.K. Song, J.-W. Choi, S.H. Yue, H. Lee, B.-K. Na, Catal. Today 89 (2004) 27–33.
[17] C.-j. Liu, G.H. Xu, T. Wang, Fuel Process. Technol. 58 (1999) 119–134.
[18] Q. Wang, B.-H. Yan, Y. Yin, Y. Cheng, Plasma Chem. Plasma Process. 29 (2009) 217–228.
[19] C.-j. Liu, B. Xue, B. Eliasson, F. He, Y. Li, G.-H. Xu, Plasma Chem. Plasma Process 21 (2001) 301–310.
[20] X. Tao, M. Bai, X. Li, H. Long, S. Shang, Y. Yin, X. Dai, Prog. Energy Combust. Sci. 37 (2011) 113–124.
[21] Q. Wang, H. Shi, B. Yan, Y. Jin, Y. Cheng, Int. J. Hydrogen Energy 36 (2011) 8301–8306.
[22] R. Snoeckx, R. Aerts, X. Tu, A. Bogaerts, J. Phys. Chem. C 117 (2013) 4957–4970.
[23] C. De Bie, T. Martens, J. Van Dijk, S. Paulussen, B. Verheyde, S. Corthals, A. Bogaerts, Plasma Sources Sci. Technol. 20 (2011) 024008.

[24] Z. Bo, J. Yan, X. Li, Y. Chi, K. Cen, Int. J. Hydrogen Energy 33 (2008) 5545–5553.
[25] M. Jasiński, M. Dors, J. Mizeraczyk, J. Power Sources 181 (2008) 41–45.
[26] Y.-F. Wang, C.-H. Tsai, W.-Y. Chang, Y.-M. Kuo, Int. J. Hydrogen Energy 35 (2010) 135–140.
[27] M.B. Lee, Q.Y. Yang, S.L. Tang, S.T. Ceyer, J. Chem. Phys. 85 (1986) 1693.
[28] Q.Y. Yang, K.J. Maynard, A.D. Johnson, S.T. Ceyer, J. Chem. Phys. 102 (1995) 7734.
[29] M.P. Kaminsky, N. Winograd, G.L. Geoffroy, M. Albert Vannice, J. Am. Chem. Soc. 108 (1986) 1315–1316.
[30] B. Xing, X.-Y. Pang, G.-C. Wang, Z.-F. Shang, J. Mol. Catal. A: Chem. 315 (2010) 187–196.
[31] J. Li, E. Croiset, L. Ricardez-Sandoval, J. Mol. Catal. A: Chem. 365 (2012) 103–114.
[32] J.E. Mueller, A.C.T. van Duin, W.A. Goddard, J. Phys. Chem. C 114 (2010) 4939–4949.
[33] W. Somers, A. Bogaerts, A.C.T. van Duin, E.C. Neyts, J. Phys. Chem. C 116 (2012) 20958–20965.
[34] Y. Shibuta, R. Arifin, K. Shimamura, T. Oguri, F. Shimojo, S. Yamaguchi, Chem. Phys. Lett. 565 (2013) 92–97.
[35] A.C.T. van Duin, S. Dasgupta, F. Lorant, W.A. Goddard, J. Phys. Chem. A 105 (2001) 9396–9409.
[36] W. Somers, A. Bogaerts, A.C.T. van Duin, S. Huygh, K.M. Bal, E.C. Neyts, Catal. Today 211 (2013) 131–136.
[37] E.C. Neyts, J. Vac. Sci. Technol. B 30 (2012) 030803.
[38] E.C. Neyts, A.C.T. van Duin, A. Bogaerts, Nanoscale 5 (2013) 7250–7255.
[39] U. Khalilov, G. Pourtois, A.C.T. van Duin, E.C. Neyts, Chem. Mater. 24 (2012) 2141–2147.
[40] S. Monti, A.C.T. van Duin, S. Kim, V. Barone, J. Phys. Chem. C 116 (2012) 5141–5150.
[41] E.C. Neyts, Y. Shibuta, A.C.T. van Duin, A. Bogaerts, ACS Nano 4 (2010) 6665–6672.
[42] E.C. Neyts, A.C.T. van Duin, A. Bogaerts, J. Am. Chem. Soc. 133 (2011) 17225–17231.
[43] E.C. Neyts, A.C.T. van Duin, A. Bogaerts, J. Am. Chem. Soc. 134 (2012) 1256–1260.
[44] K. Chenoweth, A.C.T. van Duin, W.A. Goddard, J. Phys. Chem. A 112 (2008) 1040–1053.
[45] G. Bussi, D. Donadio, M. Parrinello, J. Chem. Phys. 126 (2007) 014101.
[46] C.H. Bartholomew, Appl. Catal. A: Gen. 212 (2001) 17–60.